Title page

The names of the authors: Mihoko Hoshino[1], Mitsuyoshi Kimata[2], Craig A. Chesner[3], Norimasa Nishida[4], Masahiro Shimizu[2], and Takeshi Akasaka[5]

Title: Crystal chemistry of volcanic allanites indicative of naturally induced oxidation-dehydration

The affiliations and addresses of the authors:

[1] Mineral Resource Research Group, Institute for Geo-Resources and Environment, National Institute of Advanced Industrial Science and Technology, 1-1-1 Higashi, Tsukuba, Ibaraki, 305-8567, Japan

[2] Doctoral Program in Earth Evolution Sciences, Graduate School of Life and Environmental Sciences, University of Tsukuba, Tennodai1-1-1, Ibaraki, 305-8572, Japan

[3] Department of Geology and Geography, Eastern Illinois University, Charleston, IL, 61920, USA

[4] Chemical Analysis Division, Research Facility Centre for Science and Technology, University of Tsukuba, Tennodai1-1-1, Ibaraki, 305-8577, Japan

[5] Center for Tsukuba Advanced Research Alliance, University of Tsukuba, 1-1-1 Tennodai, Tsukuba, 305-8572, Japan.

The e-mail address, telephone and fax numbers of the corresponding author:

Corresponding author: Mihoko Hoshino

E-mail: hoshino-m@aist.go.jp

Telephone numbers: +81-29-861-2474

Fax numbers: +81-29-861-3717

Introduction

Allanite [$CaREEAl_2Fe^{2+}Si_3O_{11}O(OH)$], one of the epidote-group minerals, is known as a characteristic accessory mineral in various rocks, such as granites, granodiorites, monzonites, syenites, limestone, skarns and occasionally volcanic rocks (Deer et al. 1986; Gaines et al. 1997; Gieré and Sorensen 2004). Although allanite is considered a rare mineral in volcanic rocks, it has been described in rhyolitic tuffs, ashes, obsidian, and andesites (e.g., Duggan 1976; Hildreth 1979; Brooks et al. 1981; Mitropoulos 1987; Chesner and Ettlinger 1989; Sakai and Kurokawa 2002). The crystal structure of allanite from a biotite-granite was first determined by Ueda (1955). Subsequently, crystal structures of unaltered and non-metamict allanites from granitic pegmatites have been refined (Dollase 1971; Kartashov et al. 2002; Hoshino et al. 2005), but no crystal structure of allanite from a volcanic rock has yet to be reported.

In this paper we describe the chemical composition and crystal structure of allanite crystals from both welded rocks of the Youngest Toba Tuff, Sumatra, Indonesia (YTT; 74 Ka) and volcanic ash beds in Niigata, Japan (SK100-VAB; 1.6 Ma), and comparatively discuss their formations.

Samples

The YTT sample (T-37A) was collected in the town of Prapat, inside the Toba caldera, near

the shore of Lake Toba. It is a light pink, incipiently welded tuff (undeformed pumice fragments and glass shards) with a whole rock SiO_2 content of 74.3 wt % (Chesner, personal communication). Phenocrysts consist of quartz, sanidine, andesine, biotite, amphibole, orthopyroxene, magnetite, ilmenite, fayalite, zircon and allanite. YTT allanite crystals were separated using heavy-liquid-separation techniques. Petrological and mineralogical descriptions of the Toba tuffs and other Toba allanite have been given by Chesner and Ettlinger (1989) and Chesner (1998).

Samples of the SK100 ash beds were collected along the Shibamata route, Niigata, Japan, in the early Pleistocene Uonuma Formation (Yasui et al. 1983; Kurokawa et al. 2000). Pumice fragments in the SK100-VAB contain about 68 wt% SiO_2 (Nagase and Kurokawa 1992) and consist of glass shards, andesine, biotite, orthopyroxene, augite, ilmenite, magnetite, hornblende, allanite, zircon, apatite and almandine (Kurokawa and Sakai 2001; Sakai and Kurokawa 2002; Kurokawa et al. 2004; Hoshino et al. 2007). Because the SK100-VAB has the low abundance of magnetic minerals, allanite was easily separated using a Frantz isodynamic magnetic separator.

After separation, YTT and SK100-VAB allanite grains were embedded in epoxy resin and polished. In this study, the same allanite crystals were analyzed by EMPA and X-ray diffraction (Fig. 1).

Experimental methods

Chemical composition

Chemical analyses of separated allanite grains were carried out at the Chemical Analysis Division, University of Tsukuba, using a JEOL JAX-8621 electron microprobe equipped with three wavelength-dispersion spectrometers (WDS). Qualitative analyses of allanites were made using 25 kV accelerating potential and 250 nA beam current. Qualitative analysis of fluorine and chlorine in allanite has been carried out using an accelerating voltage of 15 kV and a probe current of 1000 nA and showed both elements to be below detection limits for EMPA in all analyzed crystals. Elements detected qualitatively were included in the quantitative analyses. Quantitative analyses for major elements in the allanites were performed using an accelerating voltage of 25 kV, a beam current of 10 nA, peak count times of 10 s, background count times of 5 s, and a beam diameter of 5 μm. Concentrations of the REE in the allanites were measured using an accelerating voltage of 25 kV with a beam current 50 nA, peak count times of 20 s, background count times of 10 s, and a beam diameter of 5 μm. X-ray intensities for La, Ce, Nd were determined using the *Lα* lines, whereas the intensities for Pr and Sm peaks were measured using *Lβ* lines. As REE standards, we used synthetic Ca-Al silicate glasses containing each REE, which are available from P & G Development Ltd. The chemical

composition of the standards is given in Table 1 of Hoshino et al. (2006). The following standards, excluding the REE, were used for quantitative analyses: SiO_2 (Si$K\alpha$), TiO_2 (Ti$K\alpha$), Al_2O_3 (Al$K\alpha$), Fe_2O_3 (Fe$K\alpha$), $MnFe_2O_4$ (Mn$K\alpha$), MgO (Mg$K\alpha$), $CaSiO_3$ (Ca$K\alpha$) and ThO_2 (Th$M\alpha$). All the data were corrected with a ZAF matrix-correction program. The chemical compositions of allanites in this study used for crystal structure refinement are presented in Table 1.

Fourier-transform infrared spectroscopy

The FTIR (Varian FTS3000) study was carried out using a SPECAC, Golden Gate ATR Mk II Attenuated Total Reflection (ATR) system, under a flow of N_2 gas (prevention of influence of water vapor in the air), in order to confirm the presence and determine the content of $(OH)^-$ in allanite. The optical unit comprised a ZnSe lens, and the superior plate was equipped with a diamond ATR Mk II crystal. Under a stereomicroscope, the allanite fragments (about 50-100 μm) were completely sifted out from the polished samples with a needle with constant reference to BSE photographs prepared ahead. In order to obtain bulk spectra of allanite, a fragment of allanite placed on the diamond plate was covered with aluminum foil (thickness 11 μm) and pressurized by a sapphire anvil. Each absorbance spectrum of the about 10 μm-thick

allanite powder plate was measured in the region of 550-4000 cm^{-1} with 4 cm^{-1} resolution.

Structure refinement

The allanites from the two samples (YTT and SK100-VAB) contain apatite and/or zircon inclusions that can be seen in BSE images (Fig. 1). Under a stereomicroscope, the allanite fragments devoid of these inclusions, having the chemical compositions determined by EMPA, were completely sifted out from the polished crystals using a needle with constant reference to BSE photographs prepared ahead (Fig. 1). X-ray diffraction intensities for these single-crystal allanites were collected with a four-circle automated diffractometer (Rigaku AFC7R) with graphite-monochromated Mo$K\alpha$ radiation and rotating anode generator at the Center for Tsukuba Advanced Research Alliance, University of Tsukuba. For each allanite fragment, 25 reflections in the range $8° \leq 2\theta \leq 30°$ were collected, and the unit-cell dimensions (Table 2) were refined from the resultant setting angles using the least-squares technique. Intensity data were collected in the ω-2θ scan-mode at affixed scan-rate of 4.0° 2θ/min. All reflections were measured within the range of $5° \leq 2\theta \leq 60°$. The reflection data were corrected for Lorentz and polarisation effects, averaged and reduced to structure factors; about 1350 unique reflections [$F_0 \geq 4\sigma(F_0)$] were observed. The SHELXL-97 (Sheldrick 1997) program was used throughout this work.

Results

Chemical composition

The EMPA data demonstrate that Ce is predominant over other REE in all of the analyzed allanites, which were thus identified as allanite-(Ce) (Table 1). YTT and SK100 volcanic allanites have minimal variation in their chemical composition (Fig. 1 and Table 1). They are LREE-enriched with Ce_2O_3 up to 9.96 wt%, La_2O_3 up to 6.85 wt% and are abundant in other REE elements as well (Nd_2O_3 up to 3.74 wt%, Pr_2O_3 up to 1.43 wt%, Sm_2O_3 up to 0.66 wt%). YTT allanites have higher Mg, Ti and Th contents than SK100-VAB ones (Table 1).

Fourier-transform infrared spectroscopy

For the determination of H_2O contents in YTT and SK100-VAB allanites unaltered and non-metamict allanite from the Daibosatsu granitic pegmatite, having an approximately homogeneous chemical composition (Hoshino et al. 2005), was collected as a standard for FTIR-ATR analysis. H_2O content in the Daibosatsu allanite was determined as 1.47 wt% by a Thermogravimetry-Mass Spectrometry (TG-MS) analysis (Table 3). The obtained absorbance spectra of YTT, SK100-VAB and Daibosatsu allanites are average spectra of 5 allanite fragments, respectively. The vertical axis of their spectra was normalized on a full scale of 0 to 1

(Fig. 2).

The Beer-Lambert law represents the linear relation between absorbance and sample thickness (concentration of the absorbing species) using the molar absorption coefficient (Libowitzky and Beran 2004). Thus, with respect to concentration only integrated measurements of the band area generally allowed accurate quantities for absorbance (Libowitzky and Beran 2004). The OH-stretching bands of YTT allanite (3343 cm^{-1}) are shifted to significantly higher wavenumber compared to those of SK100-VAB (3125 cm^{-1}) and Daibosatsu one (3124 cm^{-1}) (Fig. 2). This shift may be due to dehydration of YTT allanite. The molar absorption coefficients of YTT and SK100-VAB allanites may be slightly different, but there is no detailed report concerning molar absorption coefficients of allanite. Therefore, it was assumed that the molar absorption coefficients of YTT, SK100-VAB and Daibosatsu allanites are almost identical. The H_2O contents in the YTT and SK100-VAB allanites were determined by comparing the area ratio of the $(OH)^-$ absorbance spectra of the YTT and SK100-VAB ones with that of Daibosatsu allanite containing 1.47 wt% H_2O. The measurement ranges of the integrated areas are as follows: (1) 3566-3121 cm^{-1} (OH peak) and 1145-1021cm^{-1} (reference Si-O peak) for the YTT, (2) 3498-2791cm^{-1} and 1118-1005 cm^{-1} for the SK100-VAB and (3) 3498-2791cm^{-1} and 1118-1005 cm^{-1} for the Daibosatsu (Fig. 2 and Table 3). The Si-O peak commonly observed among these three samples was used as a reference peak in order to

mediate the small differences in thickness and amount among them. The area ratio was calculated as the ratio of the area of the OH bands to that of the Si-O stretching bands for each allanite. On the basis of the standard that the OH area ratio of Daibosatsu allanite containing 1.47 wt% H_2O is 2.43, H_2O contents in YTT and SK100-VAB allanites were determined to be 0.64 and 1.65 wt% H_2O, respectively (Table 3).

Structure refinement

The refined crystal structure data for YTT and SK100-VAB allanites include the following: final atomic coordinates, isotropic and anisotropic displacement parameters (Tables 4 and 5), selected interatomic distances (Table 6), and bond valence analyses (Table 7). Refined site occupancies of these allanites are shown in the footnotes of Tables 4 and 5. The crystal structures were refined in the space group $P2_1/m$, using the structural parameters provided by Dollase (1971). Based on the vast array of chemical composition data for epidote-group minerals, Armbruster et al. (2006) suggested the re-normalization of Si = 3 if Si is >3.05 apfu. Since the structural formula of the YTT allanite has Si = 3.04, we did not renormalize. Following the previous studies of epidote-group minerals (Dollase 1971; Kartashov et al. 2002; Hoshino et al. 2008: Bonazzi et al. 2009), the structure refinement of YTT allanite was done with Si assigned only to tetrahedral sites. According to Armbruster et al. (2006), if Si<3.00 apfu,

Al is incorporated into the Si3 site. Because SK100-VAB allanite contains 0.965 Si in Si3, 0.035 Al was assigned to the site as well.

On the basis of the representative EMPA data (Table 1), (Ca+ Fe + Mn) were assigned to the A1 site, and (La + Ce + Pr + Nd + Sm + Th + Ca) to the A2 site (Tables 4 and 5). The smallest M2 octahedron has a strong preference for Al, whereas the occupancy of M1 and M3 depends on competing ions, with the cations of larger ionic radii mainly ordered on the larger M3 octahedron (e.g., Bonazzi et al. 2009). According to Bonazzi and Menchetti (1994), M2 in annealed allanite shows a lesser Fe^{3+} incorporation, while M2 in untreated one is only occupied by Al. Therefore, occupancies of M1 and M2 sites in YTT and SK100-VAB allanite were refined independently without constraints on the following positions: Al vs. Fe (M1), Al vs. Fe (M2). However, the occupancies of Ti in M1 and (Fe + Mg) in M3 were assigned using the representative EMPA values (Tables 1 and 6). The result of structural refinement of YTT allanite suggests that a small amount of Fe^{3+} is incorporated in M2 (Table 4). This incorporation corresponds to the crystal structures of annealed allanites refined by Bonazzi and Menchetti (1994) and Bonazzi et al. (2009).

Discussion

A series of reactions including the oxidation of Fe^{2+} into Fe^{3+}, the release of H_2, and the

concomitant replacement of OH^- by O^{2-}, would lead to the formation of an oxy-equivalent of allanite, namely oxyallanite. The reaction $Fe^{2+} + OH^- \leftrightarrow Fe^{3+} + O^{2-} + 1/2H_2$ is equivalent to the oxidation reaction observed in other hydrous Fe^{2+}-bearing silicate minerals, such as mica and amphibole (Hogg and Meads 1975; Ferrow 1987; Popp et al. 1995). In contrast to micas and amphiboles, the $(OH)^-$ group in allanites is bonded to the A2 and M2 sites, where the A2 site is filled almost entirely with heterovalent cations (e.g., REE^{3+}, Th^{4+}, Ca^{2+}), and M2 site with Al^{3+} (e.g., Dollase 1971). None of cations in these sites is involved in the oxidation reaction, but a small amount of Fe^{3+} is contained in the M2 site of YTT allanite (Table 4). Dollase (1973) heated natural allanites from a granitic pegmatite in air at different temperatures and analyzed Fe^{3+}/Fe_{tot} of the run products with ^{57}Fe Mössbauer spectroscopy. The Fe^{2+} contents decreased steadily above 400°C until the sample reached an almost complete oxidation state at about 700°C (Dollase 1973). By heating single crystals of allanite from granite, Bonazzi and Menchetti (1994) verified that oxidation-dehydrogenation of allanite begins at about 600°C and is complete at about 700-725 °C. Bonazzi et al. (2009), annealing the allanite-subgroup minerals in Mn silicate rock from 400 to 900 °C, suggested that all their geometrical and structural variations mark the development of an oxidation-dehydration reaction. Structural data of YTT and SK100-VAB allanites have been compared with those of allanites in Dollase (1973) and Bonazzi and Menchetti (1994), because the allanite subgroup minerals in Bonazzi et al. (2009)

and the here studied allanites (YTT and SK100-VAB) have very different composition. Unit-cell parameters of allanite from the welded YTT are distinct from those of allanite from the unwelded SK100-VAB (Table 2) by a longer *c*-axis and a larger β value. This variation is similar to the results observed in the previous heating experiments of Dollase (1973), Bonazzi and Menchetti (1994) and Bonazzi et al. (2009). The parameters *c* and β of SK100-VAB allanite correspond to those of untreated allanite in Dollase (1973) and Bonazzi and Menchetti (1994), whereas those of the YTT allanite are comparable to those annealed to 680 °C (Dollase 1973) and 800 °C (Bonazzi and Menchetti 1994) (Fig. 3).

According to Bonazzi and Menchetti (1994), the loss of H compensating the oxidation of Fe^{2+} and Mn^{2+} is made evident by a dramatic lengthening of the donor-acceptor (O10-O4) distance. Moreover, most of the lengthening occurs between 600 and 725 °C in allanite (Fig. 5 in Bonazzi and Menchetti 1994). The O10-O4 distance (3.176 Å) of YTT allanite is similar to that of the allanite annealed up to 800 °C (3.174 Å) in Bonazzi and Menchetti (1994), but these allanites have different chemical compositions. Based on the O10-O4 data and temperature of Bonazzi and Menchetti (1994), YTT allanite may have been annealed up to 800 °C. The eruption temperatures determined from Fe-Ti oxides for the entire compositional range of the YTT (68-77 wt% SiO_2) vary between 701 and 780 °C (Chesner 1998), but a Fe-Ti oxide temperature was not determined for the YTT sample in this study (T-37A). Thus, it is possible

that the YTT allanite remained at elevated temperatures (in the range suggested by Fig. 3) during the welding sufficiently long for the post-crystallization oxidation reaction process to take place. The loss of H coincident with the oxidation of both Fe^{2+} and Mn^{2+} is apparent from the lengthening of the donor-acceptor (O10-O4) distance (Bonazzi and Menchetti 1994), which is greater for YTT allanite than it is for SK100-VAB allanite (Table 6). Moreover, the bond valence sums of O4 (acceptor oxygen for H atom) and O10 (donor oxygen for H atom) are 1.962 and 1.709 v.u. for YTT allanite and 1.754 and 1.271 v.u. for SK100-VAB allanite, respectively (Table 7). The differences in bond valence sum are 0.208 v.u. for O4 and 0.438 v.u. for O10, respectively, between YTT allanite and SK100-VAB allanite. These differences account for the observation that all of the M1-O4, M3-O4, A2-O10 and M2-O10 bond distances in YTT allanite shorten markedly compared to those in the SK100-VAB allanite to satisfy the bond-valence requirements of O4 and O10 (Tables 6 and 7). This shortening suggests that the bond valences of O10 and O4 are compensated by both oxidation of divalent cations and dehydration in the YTT allanite. Moreover, the difference from the ideal total bond valence value (4.00 v.u.) of O4 and O10 in YTT allanite (0.33 v.u.) is smaller than that in SK100-VAB (0.98 v.u.). These difference values are also broadly consistent with the corresponding differences in OH content between the YTT (OH: 0.40 apfu.) and SK100-VAB allanites (OH: 1.00 apfu.) determined by FTIR- ATR (Tables 1 and 7). These refined crystal structures and

FTIR-ATR data imply that YTT allanite is basically similar to experimentally-produced oxyallanite, that is to say, YTT allanite is oxyallanite.

Based on chemical analyses of some allanite groups, Grew et al. (1991) proposed that the coupled substitution $(Fe, Mg, Mn)^{2+} + (OH)^{-1} \leftrightarrow (Al, Fe)^{3+} + O^{2-}$ is important for numerous chemical compositions of natural allanite, dissakisite and dollaseite. The presence of an oxyallanite in natural members of the epidote groups is difficult to verify because of both analytical uncertainties and the difficulty in quantitative measurement of H_2O contents in microcrystals (Gieré and Sorensen 2004). The Fe^{3+} substitution ($^{M3}Fe^{2+} + {}^{O10}OH^{-} \leftrightarrow {}^{M3}Fe^{3+} + {}^{O10}O^{2-} + 1/2H_2$) in oxyallanite has been achieved experimentally (Dollase 1973; Bonazzi and Menchetti 1994), but it has never been documented in nature (Armbruster et al. 2006). Chemical analyses, FTIR-ATR and crystal structure refinement of YTT allanites yielded the following crystal chemical formula: $(Ca_{0.83}Mn^{2+}_{0.06}Fe^{2+}_{0.11})(La_{0.24}Ce_{0.32}Pr_{0.04}Nd_{0.11}Sm_{0.02}Th_{0.04}Ca_{0.21})(Al_{0.73}Fe^{3+}_{0.19}Ti_{0.08})(Al_{0.89}Fe^{3+}_{0.11})(Fe^{2+}_{0.22}Fe^{3+}_{0.62}Mg_{0.16})(SiO_4)Si_2O_7O_{1.6}(OH)_{0.4}$. YTT allanite in this study corresponds to oxyallanite because above 50 % OH is released from the premineral. Therefore, this study proposes that natural oxyallanite may be detected by a combination of quantitative EMPA, FTIR-ATR, and crystal structure refinement and that oxyallanite might occur in silicic rocks that experienced welding at high temperatures (> 700 ºC).

Acknowledgments

We thank K. Kurokawa (Niigata University, Japan) for providing samples of SK100 volcanic ash. The paper benefited greatly from official reviews done by M. Nagashima and P. Bonazzi. We thank T. Sugaya (Systems Engineering Inc.) for his help with the FTIR-ATR. This work was funded in 2008 by the Hayashi Memorial Foundation for Female Natural Scientists.

References

Armbruster T, Bonazzi P, Akasaka M, Bermanec V, Chopin C, Gieré R, Heuss-Assbichler S, Liebscher A, Menchetti S, Pan Y, Pasero M (2006) Recommended nomenclature of epidote-group minerals. Eur J Mineral 18:551-567

Bonazzi P, Holtstam D Bindi L, Nysten P, Capitani G (2009) Multi-analytical approach to solve the puzzle of an allanite-subgroup mineral from Kesebol, Västra Götaland, Sweden. Am Mineral 94:121-134

Bonazzi P, Menchetti S (1994) Structural variations induced by heat treatment in allanite and REE-bearing piemontite. Am Mineral 79:1176-1184

Brese NE, O'Keeffe M (1991) Bond-valence parameters for solids. Acta Cryst B47:192-197

Brooks CK, Henderson P, Rønsbo JG (1981) Rare-earth partition between allanite and

glass in the obsidian of Sandy Braes, Northern Ireland. Mineral Mag 44:157-160

Chesner CA, Ettlinger AD (1989) Composition of volcanic allanite from the Toba Tuffs, Sumatra, Indonesia. Am Mineral 74:750-758

Chesner CA (1998) Petrogenesis of the Toba Tuffs, Sumatra, Indonesia. J Petrol 39:397-438

Deer WA, Howie RA, Zussman J (1986) Allanite. In Rock-forming Minerals. 2nd ed., vol. 1B, Longman Scientific and Technical Press, Essex, England, pp 151-179

Dollase WA (1971) Refinement of the crystal structures of epidote, allanite and hancockite. Am Mineral 56:447-464

Dollase WA (1973) Mössbauer spectra and iron distribution in the epidote-group minerals. Z Kristallogr 138:4l-63

Duggan MB (1976) Primary allanite in vitrophyric rhyolites from the Tweed Shield Volcano, north-eastern New South Wales. Mineral Mag 40:652-653

Ferrow E (1987) Mössbauer and X-ray studies on the oxidation of annite and Ferriannite. Phys Chem Mineral 14:270-275

Gaines RV, Skinner HCW, Foord EE, Mason B, Rosenzweig A (1997) Epidote group. In: Dana's New Mineralogy (8th ed.). John Wiley & Sons, New York, pp. 1195-1205

Gieré R, Sorensen SS (2004) Allanite and other REE-rich epidote-group minerals. In Liebscher A, Franz G (eds) Epidotes. Rev Mineral Geochem 56:431-493

Grew ES, Esssene EJ, Peacor DR, Su S-C, Asami M (1991) Dissakisite-(Ce), a new member of the epidote group and the Mg analogue of allanite-(Ce), from Antarctica. Am Mineral 76:1990-1997

Hildreth W (1979) The Bishop Tuff: evidence for the origin of compositional zonation in silicic magma chambers. Geol Soc Am Spec Paper 180:43-75

Hogg CS, Meads RE (1975) A Mössbauer study of thermal decomposition of biotites. Mineral Mag 40:79-88

Hoshino M, Kimata M, Nishida N, Kyono A, Shimizu M, Takizawa S (2005) The chemistry of allanite from the Daibosatsu Pass, Yamanashi, Japan. Mineral Mag 69:403-423

Hoshino M, Kimata M, Shimizu M, Nishida N, Fujiwara T (2006) Allanite-(Ce) in granitic rocks from Japan: Genetic implications of patterns of REE and Mn enrichment. Can Mineral 44:45-62

Hoshino M, Kimata M, Shimizu M, Nishida N (2007) Minor-element systematics of fluorapatite and zircon inclusions in allanite-(Ce) of felsic volcanic rocks from three orogenic belts: implication for the origins of their host magmas. Can Mineral

45:1337-1353

Hoshino M, Kimata M, Shimizu M, Nishida N (2008) Crystal chemical significance of chemical zoning in dissakisite-(Ce). Phys Chem Mineral 35:59-70

Kartashov PM, Ferraris G, Ivaldi G, Sokolova E, McCammon CA (2002) Ferriallanite-(Ce), $CaCeFe^{3+}AlFe^{2+}(SiO_4)(Si_2O_7)O(OH)$, a new member of the epidote group: description, X-ray and Mössbauer study. Can Mineral 40:1641-1648

Kurokawa K, Hiwatari H, Ohashi R, Noguchi M (2000) The SK110 and SK100 ash beds found from the Taira Formation in the Niitsu Hill and Kamo area, Niigata Prefecture, central Japan. Earth Sci 54: 342-347 (in Japanese)

Kurokawa K, Sakai H (2001) Tephra marker beds in the Uonuma Group along the Shibanomata route in the Niigata backarc basin, central Japan. Memoirs of the Faculty of Education and Human Sciences (Natural Sciences), Niigata University, 3:73-119 (in Japanese with English abstract)

Kurokawa K, Yahagi H, Tan M, Nagahashi Y (2004) Correlation of the Km2 tephra bed in the Kitaura Formation in the Oga Peninsula, Akita region to the SK100 tephra bed in the Niigata region, northeast Japan. Earth Sci 58:345-350 (in Japanese with English abstract)

Libowitzky E, Beran A (2004) IR spectroscopic characterization of hydrous species in

minerals. In: Beran A, Libowitzky E (eds) Spectroscopic Methods in Mineralogy, 6, EMU Notes in Mineralogy, Eötvös University Press, Budapest, pp 227-279

Nagase M, Kurokawa K (1992) Subaqueous ash flow deposit as an indicator of paleotopography: a case study of the SK110 and SK100 ashes in the Uonuma Group, Niigata region, central Japan. Geol Soc Japan, Mem 37:261-275 (in Japanese with English abstract)

Mitropoulos P (1987) Primary allanite in andesitic rocks from the Poros Volcano, Greece. Mineral Mag 51:601-604

Popp RK, Virgo D, Yoder HS, Hoering TC, Phillips MW (1995) An experimental study of phase equilibria and Fe oxy-component in kaersutitic amphibole: implications for f_{H2} and a_{H2O} in the upper mantle. Am Mineral 80:534-548

Sakai H, Kurokawa K (2002) Correlation of the Early Pleistocene SK110 and SK100 ash beds in Niigata region to the Kd25 and Kd24 ash beds in Boso Peninsula, central Japan. Earth Sci 56:217-230 (in Japanese with English abstract)

Sheldrick GM (1997) SHELXL-97, a program for crystal structure refinement. University of Göttingen, Germany

Ueda T (1955) The crystal structure of allanite, $OH(Ca,Ce)_2(Fe^{3+},Fe^{2+})Al_2OSi_2O_7SiO_4$.

Memoirs of the College of Science, University of Kyoto, Series B 22:145-163

Yasui S, Kobayashi I, Tateishi M (1983) Stratigraphy of the Uonuma Formation in the Hachikoku oil field and the southern part of Chuo oil field, Niigata Prefecture, central Japan. Earth Sci 37:22-37 (in Japanese with English abstract)

table 1
Click here to download table: Table1.xls

Table 1 Chemical composition (wt %) of single-crystal allanites[a]

Sample	YTT [d]	SK100-VAB[e]
n[b]	5	5
SiO_2	32.17 (59)[c]	31.50 (40)
TiO_2	1.13 (3)	0.78 (1)
Al_2O_3	14.67 (22)	16.20 (23)
FeO[f]	17.22(12)	16.01 (12)
MnO	0.71 (12)	0.70 (9)
MgO	1.13 (31)	0.69 (7)
CaO	10.32 (3)	10.21 (23)
La_2O_3	6.85 (25)	6.40 (26)
Ce_2O_3	9.27 (41)	9.96 (10)
Pr_2O_3	1.14 (5)	1.43 (7)
Nd_2O_3	3.27 (7)	3.74 (1)
Sm_2O_3	0.64 (11)	0.66 (6)
ThO_2	1.85 (13)	0.94 (5)
H_2O (calc)	-	1.59[n]
H_2O (meas)	0.64[g]	1.65[g]
Total	101.01	100.87
	Formula proportions of cations	
Si	3.024 (14)	2.965(10)
Ti	0.080 (1)	0.054(1)
Al	1.624 (9)	1.797(14)
Fe^{3+}	0.920 (8)	0.361(4)
Fe^{2+}	0.332 (8)	0.859(4)
Mn^{2+}	0.057 (8)	0.055 (8)
Mg	0.158 (5)	0.097 (2)
Ca	1.039 (4)	1.030 (5)
La	0.237 (4)	0.222 (9)
Ce	0.319 (7)	0.343 (5)
Pr	0.039 (1)	0.049 (3)
Nd	0.110 (1)	0.126 (2)
Sm	0.021 (2)	0.021 (2)
Th	0.040 (2)	0.020 (2)
Σ cations	8.000	8.000
OH	0.400	1.000

[a] These single crystals were used for FTIR and structure refinement

[b] *n* : number of analyzed points

[c] Number in parenthesis is standard deviation

[d] Chemical formula of YTT allanite was calculated based on 8 cations. The propotions of Fe^{2+} and Fe^{3+} were determined by maintaining charge balance between cations and anions.

[e] Fe^{2+}/Fe^{3+} of SK100-VAB allanite was calculated based on 8 cations and 12.5 atoms of oxygen

[f] Total Fe as FeO for YTT and SK100-VAB allanite

[g] Amount of H_2O was determined by FTIR-ATR

[h] Calculated by stoichiometry

table 2
Click here to download table: Table2.xls

Table 2 Details on data collection and structure refinement of allanites

Diffractometer	Rigaku AFC7R	
Wavelength	Mo*K* α radiation (λ=0.71069Å)	
Temperature	296 K	
Scan mode	*ω-2θ* scans	
Absorption correction	*Ψ* scans	
Sample name	YTT	SK100-VAB
a (Å)	8.898(4)	8.891(2)
b (Å)	5.679(3)	5.738(1)
c (Å)	10.370(4)	10.096(2)
β (°)	115.66(3)	114.69(1)
V (Å^3)	472.4(2)	468.0(1)
Space group	$P2_1/m$	$P2_1/m$
Z	2	2
Crystal size (mm)	0.05×0.05×0.05	0.05×0.05×0.05
Collected reflections	4058	5625
Unique reflections	1857	1494
R_{int} value (%)	3.00	9.00
Observed reflections $F_0 > 4\sigma(F_0)$	1348	1390
F(000)	543.2	542.0
R value (%)	3.64	4.25
R w value (%)	10.80	11.71
Goodness of fit	1.03	1.07
μ (mm^{-1})	7.4	7.25
Weighting scheme	$\omega = 1/[\sigma^2(Fo^2) + (0.0413P)^2 + 2.15P]$ where $P=(Fo^2 + 2Fc^2)/3$	$\omega=1/[\sigma^2(Fo^2) + (0.0839P)^2 + 0.93P]$ where $P=(Fo^2 + 2Fc^2)/3$
Largest diffraction peak and hole (e/Å^3)	1.53, -1.52	4.26, -2.24

table 3
Click here to download table: Table3.xls

Table 3 Relationship between the integrated area ratios of two OH absorbance bands and the H_2O contents of allanites.

	A[a]	B[b]	H_2O (wt%)
YTT	1.06	-	0.64
SK100-VAB	-	2.73	1.65
Daibosatsu	-	2.43	1.47 [c]

[a] an integrated area ratio of YTT allanite: A= 3566-3121cm-1 (OH peak) / 1145-1021 cm-1 (reference peak)

[b] an integrated area ratio of SK100-VAB and Daibosatsu: B= 3498-2791cm^{-1} (OH peak) / 1118-1005 cm^{-1} (reference peak)

[c] 1.47 wt% was determined by the following method: TG-MS measurements from 150 to 1000 °C were carried out using a SHIMAZU-TG-40 and SHIMAZU-GC/MS QP2010 for Daibosatsu allanite powder (103.8 mg) under a flow of He gas with a heating rate of 10 °C/min

table 4
Click here to download table: Table4.xls

Table 4 Atomic coordinates, isotropic and anisotropic displacement parameters ($Å^2$) of YTT allanite

Atom	*x*	*y*	*z*	U_{11}	U_{22}	U_{33}	U_{12}	U_{13}	U_{23}
A1	0.7628(2)	0.75	0.1491(2)	0.0098(2)	0.0134(2)	0.0079(2)	0	0.0031(2)	0
A2	0.61579(6)	0.75	0.42465(5)	0.0098(2)	0.0134(2)	0.0079(2)	0	0.0031(2)	0
M1	0	0	0	0.0068(6)	0.0061(6)	0.0093(6)	-0.0001(5)	0.0024(5)	0.0007(5)
M2	0	0	0.5	0.0061(7)	0.0056(7)	0.0079(7)	0.0013(6)	0.0025(6)	-0.0000(6)
M3	0.2953(1)	0.25	0.2221(1)	0.0091(5)	0.0126(5)	0.0126(5)	0	0.0038(4)	0
Si1	0.3415(2)	0.75	0.0438(2)	0.0071(8)	0.0085(8)	0.0083(7)	0	0.0030(6)	0
Si2	0.6862(2)	0.25	0.2692(2)	0.0074(8)	0.0087(8)	0.0106(8)	0	0.0041(6)	0
Si3	0.1882(2)	0.75	0.3206(2)	0.0070(7)	0.0101(8)	0.0095(8)	0	0.0044(6)	0
O1	0.2365(4)	0.9906(7)	0.0363(4)	0.012(1)	0.012(1)	0.019(2)	0.000(1)	0.007(1)	0.001(1)
O2	0.3146(4)	0.9771(6)	0.3592(4)	0.011(1)	0.010(2)	0.017(2)	-0.004(1)	0.008(1)	-0.004(1)
O3	0.7953(4)	0.0150(7)	0.3299(4)	0.011(2)	0.010(1)	0.018(2)	-0.001(1)	-0.002(1)	0.002(1)
O4	0.0562(6)	0.25	0.1246(5)	0.006(2)	0.012(2)	0.012(2)	0	0.004(2)	0
O5	0.0472(6)	0.75	0.1519(5)	0.012(2)	0.014(2)	0.009(2)	0	0.003(2)	0
O6	0.0794(6)	0.75	0.4130(5)	0.014(2)	0.012(2)	0.011(2)	0	0.008(2)	0
O7	0.5147(6)	0.75	0.1783(5)	0.011(2)	0.015(3)	0.013(2)	0	0.002(2)	0
O8	0.5334(7)	0.25	0.3124(6)	0.015(2)	0.025(3)	0.018(3)	0	0.012(2)	0
O9	0.6152(8)	0.25	0.0943(6)	0.025(3)	0.030(3)	0.012(2)	0	0.013(2)	0
O10	0.0920(6)	0.25	0.4433(5)	0.010(2)	0.011(2)	0.017(2)	0	0.009(2)	0

Site contents: $(Ca_{0.83,}\ Mn^{2+}_{0.06,}\ Fe^{2+}_{0.11})_{\Sigma 1.00}$ for A1; $(La_{0.24}, Ce_{0.32}, Pr_{0.04}, Nd_{0.11}, Sm_{0.02}, Th_{0.04}, Ca_{0.21})_{\Sigma 0.98}$ for A2, $(Al_{0.73}, Fe^{3+}_{0.19}, Ti_{0.08})_{\Sigma 1.00}$ for M1, $(Al_{0.89}, Fe^{3+}_{0.11})_{\Sigma 1.00}$ fo
$Fe^{3+}_{0.62}, Mg_{0.16})_{\Sigma 1.00}$ for M3, $Si_{1.00}$ for Si1, $Si_{1.00}$ for Si2 and $Si_{1.00}$ for Si3

table 5
Click here to download table: Table5.xls

Table 5 Atomic coordinates, isotropic and anisotropic displacement parameters ($Å^2$) of SK100-VAB allanite

Atom	*x*	*y*	*z*	U_{11}	U_{22}	U_{33}	U_{12}	U_{13}	U_{23}
A1	0.7578(2)	0.75	0.1514(1)	0.0175(6)	0.0135(5)	0.0131(5)	0	0.0089(4)	0
A2	0.59358(4)	0.75	0.42938(3)	0.0048(2)	0.0124(2)	0.0063(2)	0	0.0010(2)	0
M1	0	0	0	0.0050(5)	0.0081(6)	0.0074(6)	-0.0007(4)	0.0016(4)	-0.0003(5)
M2	0	0	0.5	0.0048(6)	0.0078(8)	0.0085(7)	-0.0002(5)	0.0017(5)	-0.0005(6)
M3	0.3017(1)	0.25	0.21355(9)	0.0062(4)	0.0123(4)	0.0107(4)	0	0.0011(3)	0
Si1	0.3382(2)	0.75	0.0369(2)	0.0062(7)	0.0090(7)	0.0080(7)	0	0.0017(5)	0
Si2	0.6859(2)	0.25	0.2798(2)	0.0049(6)	0.0111(7)	0.0075(7)	0	0.0019(5)	0
Si3	0.1876(2)	0.75	0.3233(2)	0.0045(6)	0.0103(7)	0.0088(7)	0	0.0029(5)	0
O1	0.2332(4)	0.9883(6)	0.0257(3)	0.008(1)	0.013(1)	0.020(1)	0.002(1)	0.005(1)	0.002(1)
O2	0.3125(4)	0.9724(6)	0.3655(3)	0.008(1)	0.014(1)	0.013(1)	-0.001(1)	0.0042(9)	-0.000(1)
O3	0.7957(3)	0.0143(6)	0.3376(3)	0.007(1)	0.011(1)	0.013(1)	-0.000(1)	-0.001(1)	0.001(1)
O4	0.0569(5)	0.25	0.1292(5)	0.008(2)	0.015(2)	0.007(2)	0	0.000(1)	0
O5	0.0495(5)	0.75	0.1513(5)	0.010(2)	0.013(2)	0.008(2)	0	0.002(1)	0
O6	0.0679(5)	0.75	0.4114(5)	0.011(2)	0.010(2)	0.015(2)	0	0.009(2)	0
O7	0.5088(5)	0.75	0.1781(5)	0.009(2)	0.014(2)	0.012(2)	0	0.001(2)	0
O8	0.5416(6)	0.25	0.3332(5)	0.008(2)	0.033(3)	0.017(2)	0	0.006(2)	0
O9	0.6111(6)	0.25	0.1018(5)	0.015(2)	0.023(2)	0.007(1)	0	0.004(1)	0
O10	0.0851(5)	0.25	0.4274(4)	0.008(2)	0.012(2)	0.011(2)	0	0.005(2)	0

Site contents: $(Ca_{0.81,}\ Fe^{2+}_{0.13,}\ Mn^{2+}_{0.06})_{\Sigma 1.00}$ for A1; $(La_{0.22},\ Ce_{0.34},\ Pr_{0.05},\ Nd_{0.13},\ Sm_{0.02},\ Th_{0.02},\ Ca_{0.22})_{\Sigma 1.00}$ for A2, $(Al_{0.76},\ Fe^{3+}_{0.18},\ Ti_{0.06})_{\Sigma 1.00}$ for M1, $Al_{1.00}$ for M2, $(Fe^{2+}_{0.73.}$ $_{\Sigma 1.00}$ for M3, $Si_{1.00}$ for Si1, $Si_{1.00}$ for Si2 and $(Si_{0.96,}\ Al_{0.04})$ for Si3

table 6
Click here to download table: Table6.xls

Table 6 Selected bond lengths (Å) in the structures of allanites

	YTT	SK100-VAB		YTT	SK100-VAB
A1-O3×2	2.323(4)	2.328(3)	M3-O8	1.909(6)	1.964(5)
O7	2.355(6)	2.340(5)	O4	1.920(5)	1.979(4)
O1×2	2.425(4)	2.362(4)	O2×2	2.059(4)	2.185(3)
O5	2.519(5)	2.594(5)	3- O1×2	2.299(4)	2.293(3)
O6	2.956(6)	2.906(5)	<M3-O>	2.091	2.150
O9×2	3.076(3)	3.105(2)	No. e (M3)	23.8	24.6
<A1-O>	2.609	2.603			
No. e (A1)	21.0	21.1			
A2-O7	2.312(5)	2.325(4)	Si1-O7	1.568(6)	1.589(4)
O2×2	2.571(4)	2.466(3)	Si1-O1×2	1.638(4)	1.633(3)
O10	2.356(5)	2.608(4)	Si1-O9	1.636(6)	1.640(5)
O2×2	2.781(4)	2.635(3)	<Si1-O>	1.620	1.624
O3×2	2.672(4)	2.789(3)	No. e (Si1)	14	14
O8×2	3.036(4)	3.002(2)			
O8	3.515(1)[a]	3.100(1)[a]			
<A2-O>	2.679	2.672			
No. e (A2)	50.2	50.5			
M1-O4×2	1.837(3)	1.861(3)	Si2-O8	1.606(6)	1.586(5)
M1-O1×2	1.972(4)	1.980(3)	Si1-O3×2	1.609(4)	1.627(3)
M1-O5×2	2.025(3)	2.006(3)	Si1-O9	1.642(6)	1.635(5)
<M1-O>	1.945	1.949	<Si2-O>	1.617	1.619
No. e (M1)	16.2	15.9	No. e (Si2)	14	14
M2-O3×2	1.912(4)	1.872(3)	Si3-O2×2	1.643(4)	1.627(3)
M1-O10×2	1.857(3)	1.905(3)	Si1-O5	1.653(5)	1.656(5)
M1-O6×2	1.970(3)	1.916(3)	Si1-O6	1.631(5)	1.648(5)
<M2-O>	1.913	1.898	<Si3-O>	1.643	1.640
No. e (M2)	14.3	13	No. e (Si3)	14	14.0
O10-O4	3.176 (8)	2.915 (3)			

No. e = mean number of electrons derived from site occupancy refinement in Tables 4 and 5: the mean number of electrons was calculated according to the procedure described by Bonazzi and Menchetti (1994)

[a] The A2-O8 distances marked with asterisks are not included in the calculation of the mean value

table 7
Click here to download table: Table7.xls

Table 7 Bond-valence sums for O4 and O10

	YTT	SK100-VAB
M1-O4 (×2)	0.671	0.619
M3-O4	0.620	0.516
Total	1.962	1.754
M2-O10 (×2)	0.596	0.503
A2-O10	0.517	0.265
Total	1.709	1.271

The bond-valence parameters are from Brese and O'Keeffe (1991)

figure 1
Click here to download high resolution image

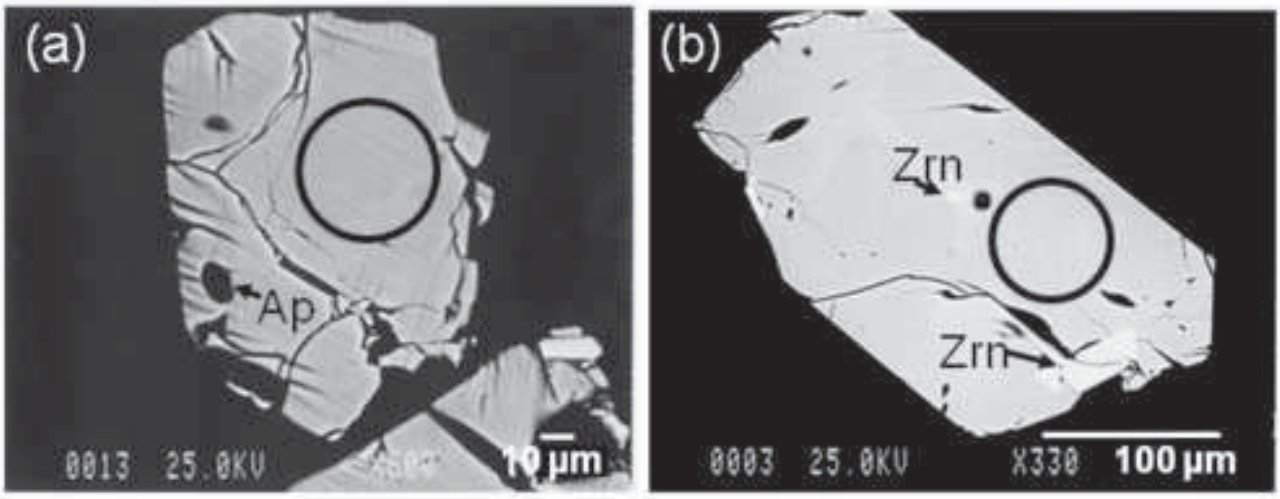

Fig. 1 Back-scattered-electron images showing representative textures of the allanite with apatite (Ap) and/or zircon (Zrn) inclusions from (a) Youngest Toba welded tuff (YTT) and (b) SK100 volcanic ash beds (SK100-VAB). Open circles denote the analytical points in Table 1. The areas are extracted from polished samples, used for FT-IR and crystal structural analysis

figure 2
Click here to download line figure: Figure 2.eps

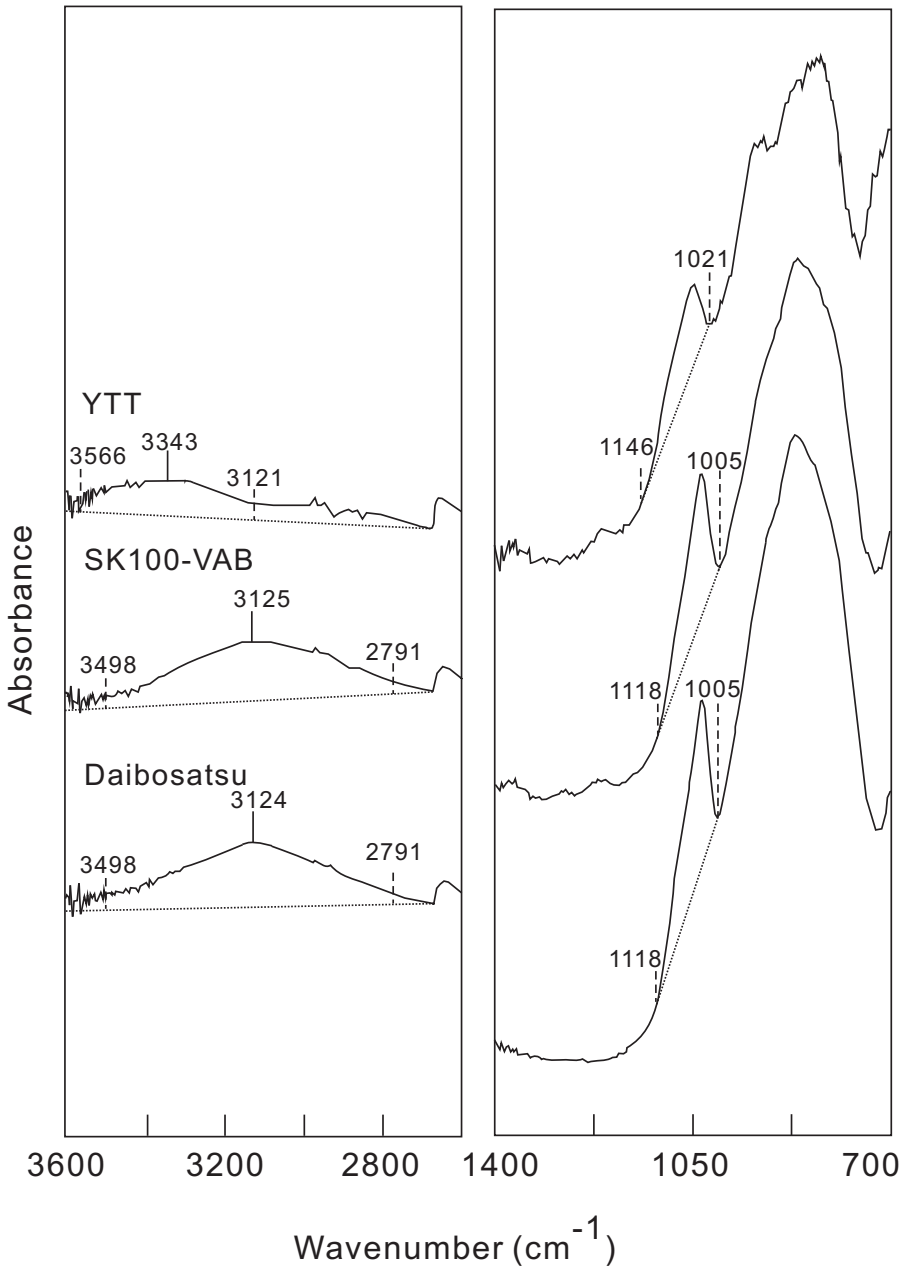

Fig. 2 FTIR-ATR spectra of the powdered allanites from Youngest Toba welded tuff (YTT), SK100 volcanic ash beds (SK100-VAB) and Daibosatsu granitic pegmatite. Dotted lines represent base lines of measurement curves for OH and reference peaks, while dashed lines show the integrated area of the absorbance peaks.

figure 3
Click here to download line figure: Figure 3.eps

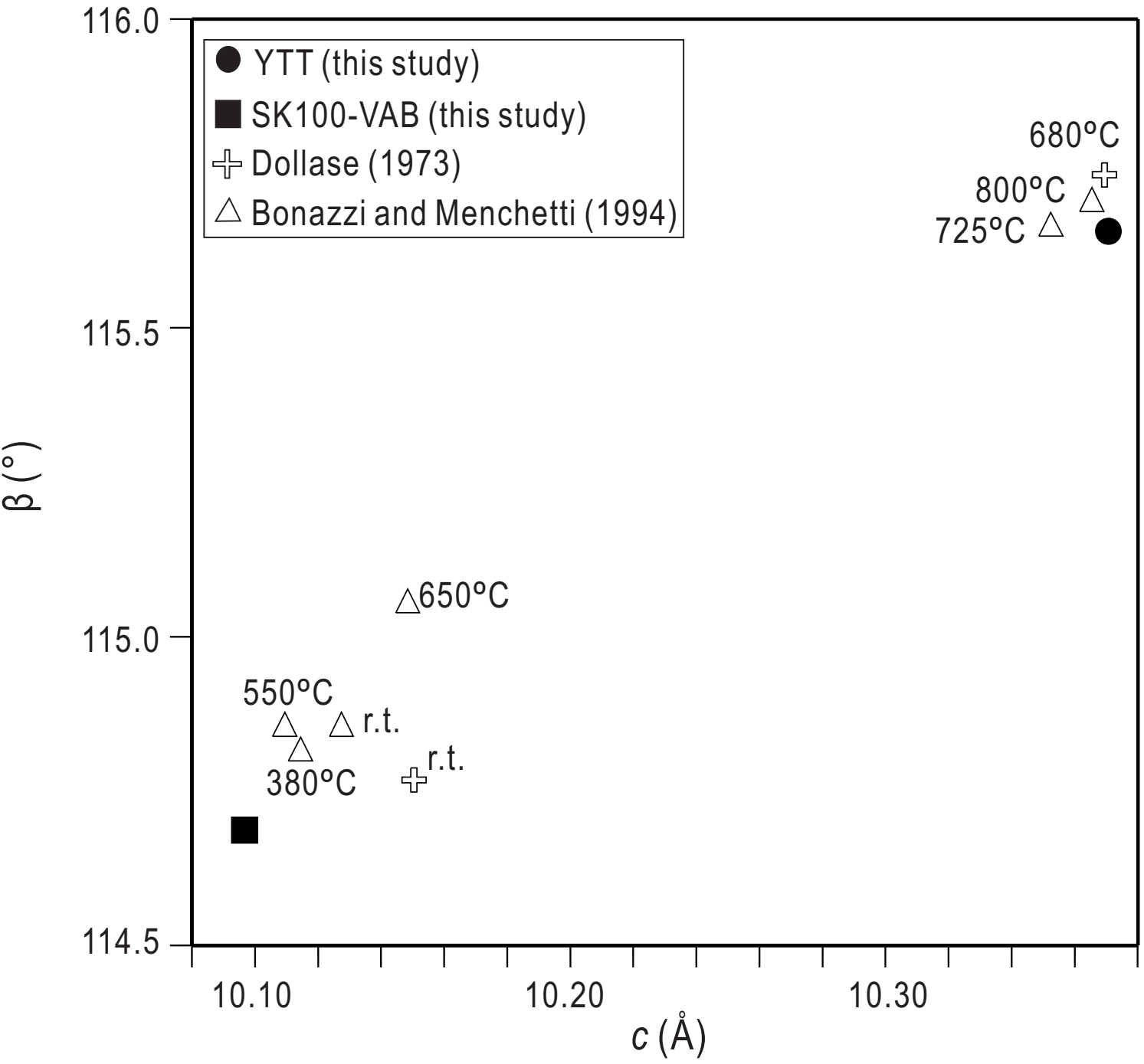

Fig. 3 *c* axis versus ß value of natural and annealed allanites